Journal of Fluids and Structures 51 (2014) 354–361

Contents lists available at ScienceDirect

Journal of Fluids and Structures

journal homepage: www.elsevier.com/locate/jfs

Experimental study of extreme thrust on a tidal stream rotor due to turbulent flow and with opposing waves

E. Fernandez-Rodriguez, T.J. Stallard *, P.K. Stansby

School of Mechanical, Aerospace and Civil Engineering, University of Manchester, Manchester M13 9PL, United Kingdom

ARTICLE INFO

Article history:
Received 26 February 2014
Accepted 17 September 2014
Available online 28 October 2014

Keywords:
Tidal stream turbines
Open channel turbulence
Waves and current

ABSTRACT

Time-varying thrust has been measured on a rotor in shallow turbulent flow at laboratory scale. The onset flow has a turbulence intensity of 12% at mid depth and a longitudinal turbulence length scale of half the depth, about 5 times the vertical scale, typical of shallow flows. The rotor is designed to have thrust and power coefficient variations with tip speed ratio close to that of a full-scale turbine. Three extreme probability distributions give similar thrust exceedance values with the Type 1 Pareto in mid range which gives 1:100, 1:1000 and 1:10 000 exceedance thrust forces of 1.38, 1.5 and 1.59 times the mean value. With opposing waves superimposed the extreme thrust distribution has a very similar distribution to the turbulent flow only. Exceedance forces are predicted by superposition of a drag force with drag coefficient of 2.0 based on the wave particle velocity only and with an unchanged mean thrust coefficient of 0.89. These values are relevant for the design of support structures for marine turbines.

1. Introduction

Tidal stream turbines are being designed to convert energy from tidal flows into electricity. Several prototype turbines have demonstrated the potential of this technology with rated power of around 1 MW. Planning is ongoing for arrays of turbines at various sites including in the Pentland Firth (Scotland), the Skerries (N Wales), the Bay of Fundy (Canada) and near Brittany (France). Most of the turbines in development are superficially similar to wind turbines, typically with a horizontal axis and two or three blades. However rotor diameter is limited by the water depth and tidal turbine blades typically have smaller aspect ratio (chord/blade length) and greater thickness due to high root bending moments. Turbulence in tidal flows is also quite different from that in wind for which an unbounded turbulent boundary layer is applicable. Tidal flows are bounded by the water surface and this causes horizontal length scales to be many times the vertical which are typically about 10% of the depth as suggested by Prandtl (1927). Horizontal length scales of about half the water depth are typical of shallow flows; for example this has been demonstrated for wakes in Stansby (2003).

The rotor and blade geometry of a tidal turbine are generally designed using blade element momentum theory, combining force coefficient versus angle of incidence for typical hydrofoil geometries with momentum theory to determine variation of power and thrust coefficient with tip speed ratio. This is quite successful and can be formulated for quasi-steady onset flows due to wave-induced kinematics and for dynamic problems such as electrical fault (Moriarty and Hansen, 2005; Bossanyi, 2007; Masters et al., 2011). Computational fluid dynamics (CFD) has provided more detailed information, particularly with regard to loading due to turbulence (Afgan et al., 2013), blockage effects (Nishino and Willden, 2013) and

* Corresponding author.
E-mail address: tim.stallard@manchester.ac.uk (T.J. Stallard).

http://dx.doi.org/10.1016/j.jfluidstructs.2014.09.012

the wake structure (Churchfield et al., 2013). Experimental studies have demonstrated the effect of unsteady onset flow on thrust, power and blade loads. Thrust variation of a constant speed turbine has been analysed due to homogenous turbulence and waves (Gaurier et al., 2013) and due to channel turbulence (Chamorro et al., 2013). However limited attention has been given to extreme loading despite the importance of this for support structures and blade design. In this study, laboratory scale experimental measurements are reported and analysed to assess extreme thrust characteristics. This also gives some indication of extreme blade loads although they are not directly measured. We consider turbulent flow over a smooth bed within a wide channel. The effect of superimposed opposing waves is also analysed. Although turbines are often shutdown with wave heights above a certain threshold smaller waves affect power generation and loading and hence extreme loading.

2. Experimental conditions

Experiments were undertaken in the wide flume at University of Manchester, 5 m wide with a water depth $h=0.46$ m giving a scale of around 1:70 compared to a tidal site of approximately 30 m depth. The mean flow speed at hub height U_0 was 0.46 m/s and the design of rotors for this laboratory scale is described below. The flume has a conventional design with deep chambers at either end connected by two large diameter pipes located beneath the flat bed and containing axial flow turbines. A vertical mesh was placed across the inlet to the horizontal bed to break up the large-scale structures resulting from jets entering a chamber. The rotor plane was located at 6.0 m from the inlet and the velocity field was analysed at this location prior to tests with the rotor installed. The rotor axis was positioned at mid-depth and mid-span.

2.1. Flow measurement

Time varying velocities were recorded using NORTEK Vectrino+ ADV probes with velocity range ± 100 cm s^{-1}, sample volume of 3 mm and transmit length of 8.7 mm. These settings returned signal to noise ratio SNR >15 dB and correlation coefficient COR $>90\%$ for the majority ($>95\%$) of samples. Velocity was sampled at 200 Hz, sufficient to resolve the channel turbulence to the dissipation range (Nezu and Nakagawa, 1993, p. 30). Probes are positioned in the cross-stream y–z plane by an automated traverse table with position accuracy of 1 mm and the carriage is located manually in the longitudinal x-axis. Longitudinal mean velocity U_0 and turbulence intensity u'_{rms}/U_0, where u' is fluctuating velocity, were obtained from samples of time-varying longitudinal velocity $u(t)$ obtained from a single probe. Longitudinal turbulence length scale L_{uu} was obtained from auto-correlation R_{uu} of the measured velocity applying the frozen turbulence assumption:

$$L_{uu} = U_0 \int_0^{\infty} R_{uu} d\tau, \tag{2.1}$$

$$R_{uu} = \frac{u'(t)u'(t+d\tau)}{u'(t)^2}. \tag{2.2}$$

The velocity profile measured at the rotor plane is shown in Fig. 1 along with the longitudinal turbulence intensity, which is fairly constant at about 12%. The length scale at mid depth is 0.267 m, or 59% of the water depth. Turbulence length scales

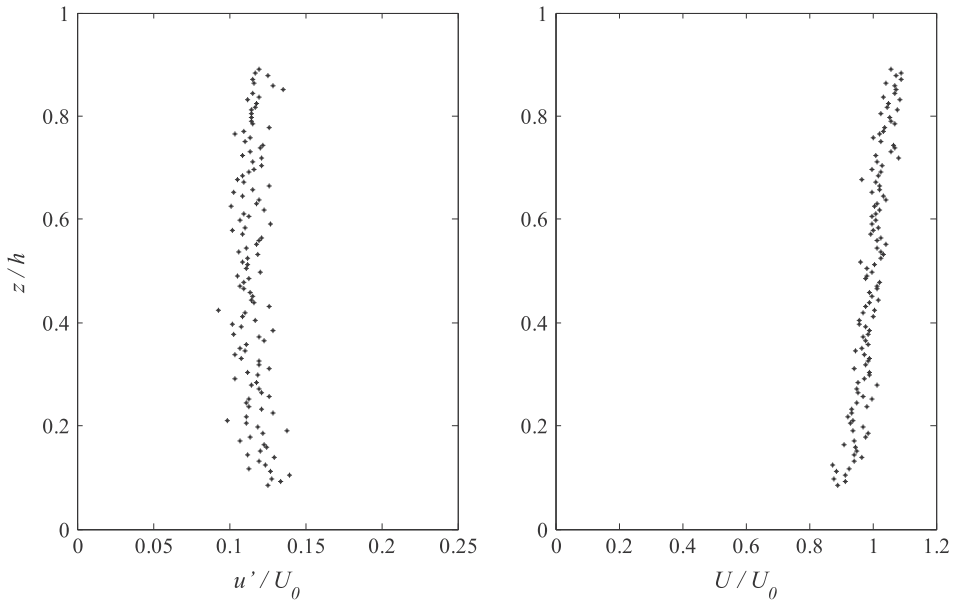

Fig. 1. Depth variation of turbulence intensity u'/U_0 and normalised mean velocity U/U_0 for channel flow at rotor axis. Obtained from 1 min samples.

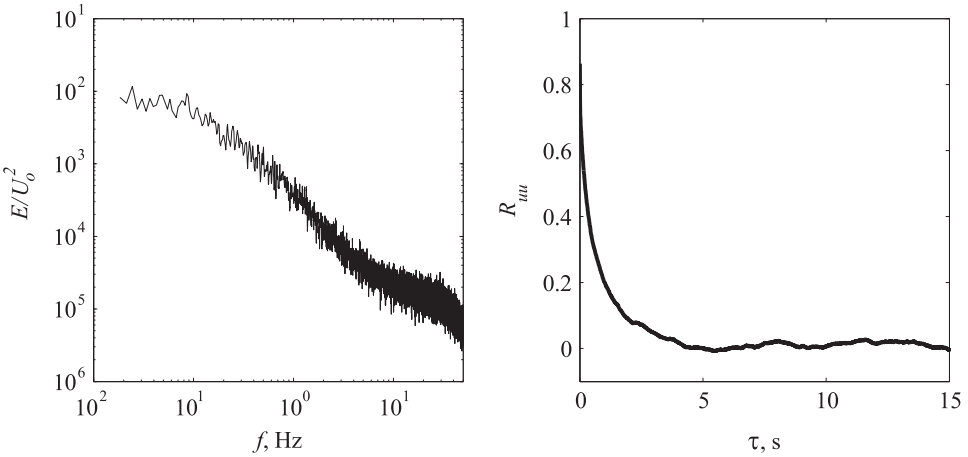

Fig. 2. Spectrum and auto-correlation function of ambient velocity at rotor axis. Turbulence intensity is 12%.

were also obtained from cross correlation between samples of 600 s duration measured simultaneously by two probes separated in the streamwise direction and results were within 5%.

The spectrum of velocity at mid-depth at the rotor plane is shown in Fig. 2 and there is energy across a range of frequencies including low frequencies down to 0.02 Hz. This is evident in the autocorrelation function shown in Fig. 2 where small magnitude periodic motion with period of around 5 s is apparent. This is associated with the large-scale horizontal structures that occur in shallow flows. Energy is prominent for the frequency range less than 0.5 Hz.

Waves were generated by sinusoidal motion of piston type wave paddles located at the outflow of the channel. The time varying free surface elevation, η, was measured at the rotor plane using three capacitance type wave gauges located at one metre spacing about the flume centreline.

2.2. Rotor thrust

The operation of a tidal stream turbine is typically characterised by the variation of thrust coefficient C_T, and power coefficient, C_P, with tip speed ratio β. A three-bladed rotor has been designed with radius $R=0.135$ m and variation of thrust coefficient with tip speed ratio close to that of a full-scale turbine. Explanation of the rotor design process is given by Whelan and Stallard (2011) and the resultant wake analysed by Stallard et al. (2013). The rotor comprised three blades formed from a Gottingen 804 foil. The foil section was selected based on the moderate chord Reynolds number of these experiments ($Re_C \approx 30\,000$ at 3/4 span at $\beta=4.5$ compared to $Re_C > 6\times10^6$ for a full-scale rotor of 18 m diameter). Lift and drag coefficients for $Re_C=20,000$ (Miley, 1982) and 30 000 (Hassan, 1993) were employed for design. The radial variation of chord length and twist angle was selected using a blade element code to develop (i) $C_T(\beta)$ variation close to- and (ii) C_P of similar magnitude to that of a representative full-scale turbine. The rotor was manufactured from a CAD geometry in one piece by the rapid prototyping method Synthetic Laser Sintering (SLS) using glass fibre reinforced polymer-acrylic (PA12-GF).

The rotor was mounted directly on the shaft of a 90° bevel gearbox with acrylic gears (Huco B332.31.3). This was attached to a 15 mm outer diameter stainless steel rod rigidly attached to a mounting plate and gantry. A 4 mm diameter driveshaft transferred mechanical torque to an encoder and motor located above the water level. Only the rotor, gearbox and lower part of the supporting shaft were immersed. The centreline of the supporting shaft was located 0.15D downstream of the rotor plane and the gearbox extended to 0.2D downstream. This configuration was employed to minimise dimensions of the immersed support structure. Thrust was measured via a full-bridge strain gauge (EA-06-125PC-350W by Micro Measurements) connected to a National Instruments SCC-SG24 strain gauge module. Strain gauges were mounted on the support shaft 800 mm above the rotor axis and calibrated by measurement of the voltage corresponding to fixed increments of load applied to the hub prior to immersion. A linear relationship was obtained between applied load and measured voltage by least-squares-best-fit. The residual was less than 0.1% in all cases. Horizontal force measured by the strain gauges is due to horizontal thrust on both the swept area of the rotor (F) and drag on the supporting structure (F_{tower}). Measurements of the force on the support structure only, i.e. without the rotor attached, indicated an average force, $F_{tower}=0.38$–0.44 N. In comparison, thrust on the rotor plane only was the order of $F\sim6$ N indicating that support structure loading was an order of magnitude smaller than the rotor thrust. The thrust coefficients reported herein were obtained after subtracting the nominal tower load so that $C_T=2F/\rho A_D U_0^2$ where A_D is rotor plane area and ρ is water density.

Angular displacement was measured using a HEDS 9000 quadrature encoder reading an HEDM 6120 T12 code wheel. The code-wheel has 2000 counts per revolution thus providing position resolution of $\pi/100$. Angular speed, ω, was obtained by differentiation of the measured angular displacement. Torque applied to the rotor was defined by a dynamometer system developed by Brown (2009). This comprised a firmware controller specifying the bridge current across a 24 V DC motor (CROUZET 82800 series) as a function of measured angular speed. The net retarding torque, Q, is the sum of mechanical

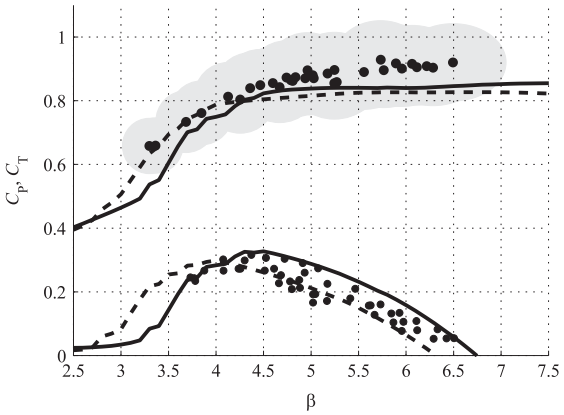

Fig. 3. Variation of thrust and power coefficient with tip speed ratio obtained from experiment (mean denoted by solid points and standard deviation of thrust for mean β and of β for mean thrust is covered by the shaded region) and by blade element momentum theory for unbounded flow using foil lift and drag coefficients from Miley (1982) (solid lines) and Hassan (1993) (dashed lines).

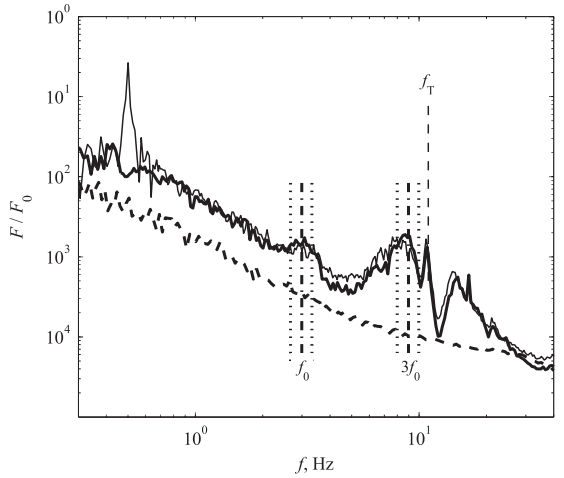

Fig. 4. Spectrum of thrust force due to turbulent flow (thick solid line) and with opposing waves of frequency 0.5 Hz (thin solid line) and of ambient flow (dashed line). Both force spectra are for mean tip speed ratio of 5.5 and vertical lines denote the mean (dash-dot line) and standard deviation (dotted line) of rotor frequency f_0 and third harmonic and the natural frequency of the support structure f_T (dashed line).

friction and motor torque where mechanical friction was defined by the motor torque that maintains constant angular speed without rotor attached.

3. Thrust due to turbulent flow

Mean values of thrust coefficient ($C_T=2F/\rho A_D U_0^2$) and power coefficient ($C_P=2Q\omega/\rho A_D U_0^3$) obtained from measurements in turbulent flow were in reasonable agreement with predictions obtained from a blade element method (GH Tidal Bladed, Bossanyi, 2007) over the range $3<\beta<7$ (where $\beta=\omega R/U_0$) as shown in Fig. 3. A constant retarding torque was applied during each sample so both angular speed and thrust varied with the onset flow with standard deviation of around 10% and 14% respectively. The thrust frequency spectrum is correlated with the energy cascade of the onset flow over low frequencies with fluctuations over a small range of frequencies close to the blade passing frequency (Fig. 4) and rotor frequency. Fluctuations are also observed close to the natural frequency of the tower and at frequencies up to 25 Hz. At higher frequencies the force spectrum tends to the onset flow spectrum.

3.1. Comparison to loading on a porous plate

In Bearman (1971) the standard deviation of drag force fluctuations experienced by a square plate in grid-generated turbulence is presented through an aerodynamic admittance $\chi^2|f|$ where $F'_{rms}/F_0 = 2\chi(f)U'_{rms}/U_0$. This was based on theory of Vickery (1965) for lattice plates. The admittance is presented as a function of fD/U_0 for different ratios of L_{uu}/D where L_{uu}

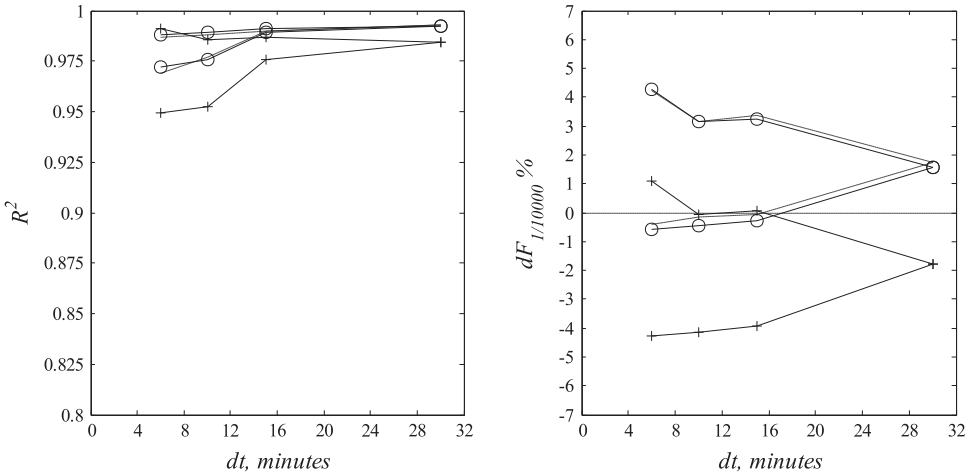

Fig. 5. Residual R^2 (left) and both maximum and minimum discrepancy $dF_{1/10\,000}$, between 1:10 000 exceedance force (right) obtained from a range of sample intervals and relative to value from 30 min interval. Data shown for Normal (+), Weibull (solid line) and Type 1-Pareto (o) probability distributions.

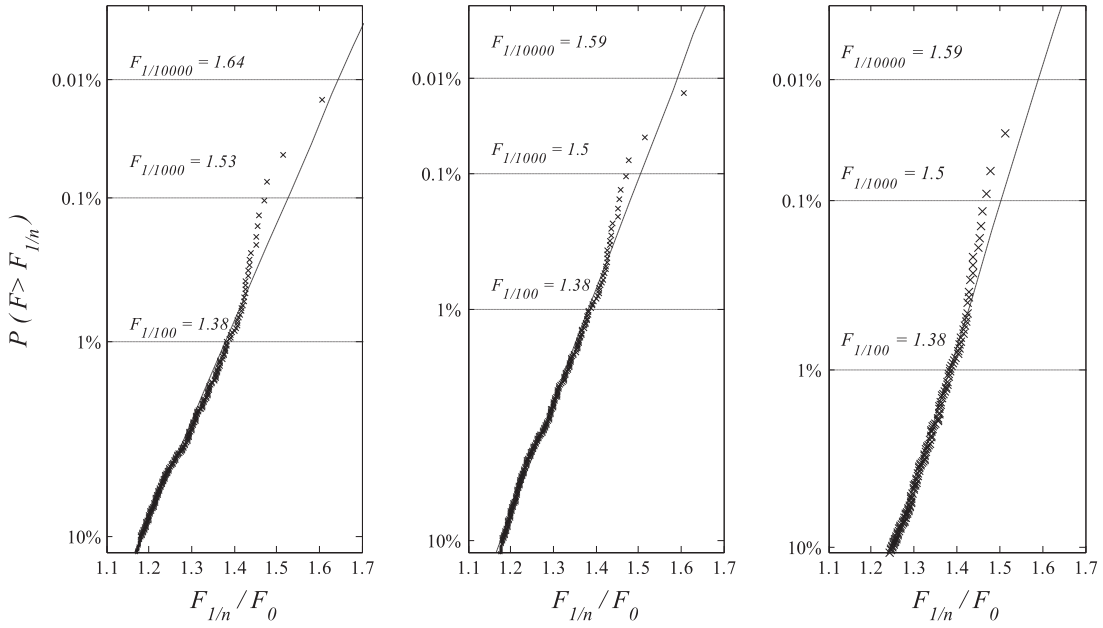

Fig. 6. Probability distribution of extreme force using normal (left), Weibull (centre) and Type 1-Pareto (right) distributions based on measurements of force due to turbulent flow with turbulence intensity of 12% and applying threshold force of 1.1 times mean thrust. F_0 is mean force.

is longitudinal length scale and D is square side length. In the present experiments the dominant frequency was less than 0.5 Hz and the ratio F'_{rms}/F_0 was measured as 14% with turbulence intensity of 12%. Applying the results for square plates shown from Bearman (1971) with $L_{uu}/D \cong 1$ for the same turbulence intensity gives an admittance of $\chi^2|f| \cong 0.56-0.84$ and corresponding F'_{rms}/F_0 of 18–22%. The difference is due the difference in shape (square and circular rotor plane), nature of the body (rigid plate and rotor) and nature of turbulence (grid and open channel).

3.2. Probability of exceedance

The measured thrust time series has been analysed to determine mean, standard deviation and exceedance forces. Independent maxima were determined and ranked in descending order. The force $F_{1/n}$ corresponding to specific exceedance probabilities $1/n$ were obtained based on normal, Weibull and Type 1 Pareto distributions. Only values above a threshold force were analysed. A threshold value and sample duration were selected such that the extreme forces were converged to within 2%. The sample interval must be large enough to provide statistically meaningful extreme value estimates. Continuous samples of 30-minute duration were analysed for intervals dt of 6, 10, 15 and 30 min. The goodness of fit R^2 with maximum and minimum values for each sample time are shown in Fig. 5 for three types of probability distribution.

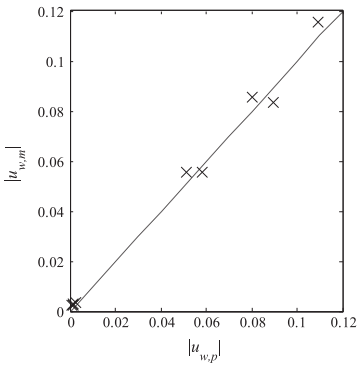

Fig. 7. Comparison of average wave-induced velocity amplitude measured at mid-depth $|u_{w,m}|$ with velocity obtained by linear theory $|u_{w,p}|$ with wave height given by $2\sqrt{2}\eta_{rms}$.

The 1:10 000 force is also plotted with maximum and minimum for each sample interval. The results show the goodness of fit is acceptable (greater than 0.95). For all three distributions the 1:10 000 thrust are within $\pm 4\%$ or $\pm 2\%$ for 15 min or 30 min intervals respectively. Thirty minutes intervals were used for further analysis and resultant probability distributions are shown in Fig. 6 with the Type 1 Pareto giving values between the Weibull and normal distributions for the 1:1000 and 1:10 000 cases. F_0 is mean force. The 1:100 case is equal for all three probability distributions and is 1.38 times the mean force. The 1:1000 and 1:10 000 forces are in the range 1.50–1.53 and 1.59–1.65 times respectively with variation due to the statistical distribution employed. The fitted distributions are close to the measured data for probability less than 1:200 with forces slightly overestimated for lower probability although agreement is close again approaching 1:10 000. This is unexplained but the Type1 Pareto is considered the preferred option.

4. Thrust due to turbulent flow with opposing waves

The Morison equation is well known and widely used for predicting forces on bodies in oscillatory flow. The drag term is typically written $F = (1/2)\,\rho\, A\, C_D\, u^2$ where u is total velocity due to the combination of turbulent flow u_c and waves u_w. Superposition of current velocity and velocity due to waves has been shown to overestimate extreme wave loads on offshore jacket structures, which may be assumed to behave as porous blocks, and this formulation has been modified in design codes for such structures (Taylor et al., 2013). A porous disc that develops a drag coefficient equivalent to the rotor thrust coefficient would have a porosity ratio (of open to total area) close to 50%. We consider the force formula where current force and wave force are superimposed as indicated by the force spectrum of Fig. 4. Force is given by

$$F = \frac{1}{2}\rho\, A\, (C_D\, u_w^2 + C_T\ u_c^2), \tag{4.1}$$

where C_D refers to the wave induced drag coefficient and C_T refers to the current induced thrust or drag coefficient. Note drag and thrust are equivalent in this context.

4.1. Kinematics

Waves were generated opposing the current with wave heights, H, up to 7 cm and wave periods, T, in the range 0.7–1.5 s. The maximum conditions correspond to about 5 m and 8 s full scale and may exceed the shutdown limit for some designs but are representative of conditions measured at test-sites (McCann et al., 2008). Regular waves were input but propagation over the turbulent current flow with large-scale horizontal structures caused some variation in wave height. Wave-induced velocity is required at hub height (mid depth) and for these cases linear theory is appropriate taking into account Doppler shifting of wave period due to average current velocity. The wave height H input to linear theory is thus $2\sqrt{2}\eta_{rms}$ giving the predicted amplitude of wave induced velocity at mid-depth as

$$|u_{w,p}| = \frac{\pi H}{T}\frac{\cosh(kh\ /2)}{\sinh(kh)} \tag{4.2}$$

where k is the wavenumber satisfying the linear dispersion relationship in water of depth h. This linear approximation is within $\pm 7\%$ of the measured amplitude of velocity with the surface elevation η measured at the same location as shown in Fig. 7.

4.2. Measured and predicted extreme thrust

Extreme forces due to turbulent flow and waves are shown in Fig. 8 for exceedance probabilities of 1:100, 1:1000, and 1:10 000. Extreme forces as measured in turbulent flow are fitted with an additional wave force defined by $(1/2)\rho u_w^2 A C_D$ for

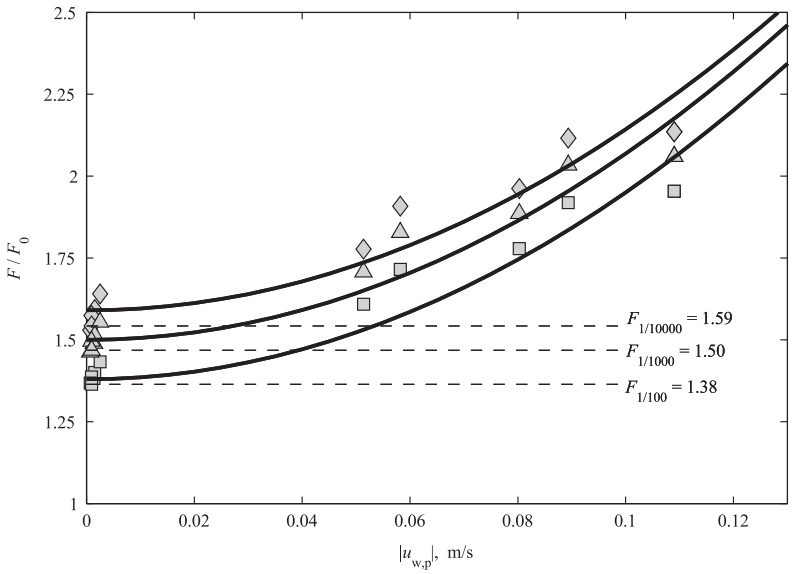

Fig. 8. Variation of 1% (□), 0.1% (Δ) and 0.01% (◇) exceedance of rotor force F/F_0 due to wave-induced velocity predicted by linear theory. Extreme forces measured due to turbulent flow only (dashed line) and predicted for turbulent flow and waves by Eq. (4.1) (solid line) are shown.

comparison. The 1:100 and 1:1000 exceedance forces are predicted within $\pm 8\%$ and $\pm 7.5\%$ with $C_D=2.0$ and the 1:10 000 case within $\pm 7\%$ with $C_D=1.97$. Overall the force is predicted by $C_D=2.0$ within $\pm 8\%$. Since the amplitude of the wave induced velocity is predicted within $\pm 7\%$ this variability is less than expected but the extreme values are due to a combination of effects and this must cause the expected variability to be reduced.

The effect of waves on extreme thrust can thus be considered as the extreme values in current alone superimposed with an oscillatory wave-induced force. In this case the thrust coefficient for current flow is 0.89 whilst that for oscillatory flow is 2.0. The latter compares with 1.1 for a thin disc in a current flow (Blevins, 2003). It is well known that drag coefficient increases for sharp edged bodies in oscillatory flow at low Keulegan Carpenter numbers, $KC=u_wT/D$, which are about 0.25–0.60 for these experiments. $C_D=2$ might be typical but will depend on KC and should be checked. The inertia force due to a rotor disc of negligible volume is small.

This force formulation was demonstrated by Taylor et al. (2013) to be effective for peak forces on lattice structures represented as porous bodies when the wave induced velocity is large in comparison with the current velocity. Here it proves to be effective when the current velocity is larger than the wave-induced velocity although this differs to formulation applied for this case by Taylor et al. (2013). Turbine power extraction and wake have long been studied by the idealised equivalence between a porous disc and a rotor in steady flow but the agreement for this combined flow is perhaps surprising. However, the wake is not quasi-steady in both cases and the probability distribution of peak forces was not considered for lattice structures. For these cases the turbulent loading on a turbine appears largely uncoupled from the oscillatory wave force presumably because the turbulence is independent of the wave-induced flow.

5. Conclusions

Thrust forces on a tidal stream rotor due to a shallow turbulent flow and with waves superimposed have been analysed to determine extreme forces. A 3-bladed fixed pitch rotor is employed for which the variation of thrust coefficient with tip speed ratio is comparable to a full-scale turbine. For turbulent flow only, the 1%, 0.1% and 0.01% exceedance forces are 1.38, 1.5 and 1.59 times the mean thrust based on a Type 1 Pareto probability distribution. This gives a good fit to data for exceedance greater than 0.5% and a reasonable fit for smaller exceedance. This indicates that measurements for longer periods are desirable to assess excedances less than 1:10 000. The standard deviation of rotor thrust due to turbulence is comparable to that on a square plate in grid generated turbulence with the same relative turbulence length scale and intensity. For flow with waves, the peak force is modelled by superposition of the force due to turbulent flow and a drag or thrust force defined by the wave-induced kinematics. Wave kinematics are not strictly sinusoidal due to interaction between waves and large-scale turbulence of the opposing flow but linear theory provides velocity at hub height to within $\pm 7\%$. Applying this force prediction method with a thrust coefficient of 2.0 provides extreme thrust forces to within $\pm 8\%$. This is within the uncertainty associated with the kinematics and this approach is of value for informing support structure design. On modern turbines power and hence thrust is controlled by pitch control of the blades based on the instantaneous onset velocity and rotor speed. This does assume that the rotor responds in a quasi-steady manner and the present results suggest this is not the case with turbulence and waves combined indicating that the strategy may need to be re-appraised.

Acknowledgements

The authors acknowledge the financial support provided to the first author by CONACYT and SEP, of the EPSRC via grant EP/J010235/1 (X-MED) and of the Performance Assessment of Wave and Tidal Array Systems (PerAWaT) project (2009-13) commissioned by the Energy Technologies Institute which supported development of experimental equipment used in this study.

References

Afgan, I., McNaughton, J., Rolfo, S., Apsley, D.D., Stallard, T., Stansby, P.K., 2013. Turbulent flow and loading on a tidal stream turbine by LES and RANS. International Journal of Heat and Fluid Flow 43, 96–108.

Bearman, P.W., 1971. An investigation of the forces on flat plates normal to a turbulent flow. Journal of Fluid Mechanics 46, 177–198.

Blevins, R., 2003. Applied Fluid Dynamics Handbook, third ed. Krieger Publishing Company, Malabar, Florida.

Brown, R.J., 2009. Design and Construction of a Dynamometer System for Testing an Array of Wave Energy Absorbers (M.Phil. dissertation). University of Manchester.

Bossanyi, E.A., 2007. GH tidal bladed theory manual. Garrad Hassan and Partners Technical Report 282/BR/009.

Chamorro, L.P., Hill, C., Morton, S., Ellis, C., Arndy, R.E.A., Sotirpoulos, F., 2013. On the interaction between a turbulent open channel flow and an axial-flow turbine. Journal of Fluid Mechanics 716, 658–670.

Churchfield, M., Li, Y., Moriarty, P., 2013. A large-eddy simulation study of wake propagation and power production in an array of tidal-current turbines. Philosophical Transactions of the Royal Society A 371, 2012.0421.

Gaurier, B., Davies, P., Deuff, A., Germain, G., 2013. Flume tank characterization of marine current turbine blade behavior under current and wave loading. Renewable Energy 59, 1–12.

Hassan, U., 1993 A wind tunnel investigation of the wake structure within small wind turbine farms. Technical Report ETSU WN 5113.

McCann, G., Thomson, M., Hitchcock, S., 2008. Implications of site-specific conditions on the predictions of loading and power performance of a tidal stream device. In: Proceedings of the 2nd International Conference on Ocean Energy, Brest, France.

Masters, I., Chapman, J.C., Orme, J.A.C., Willis, M.R., 2011. A robust blade element momentum theory model for tidal stream turbines including tip and hub loss corrections. In: Proceedings of the Institution of Marine Energy, vol. 10, 1, pp. 25–35.

Miley, S.J., 1982. A catalog of low Reynolds number airfoil data for wind turbine applications. Technical Report DE82-021712, NTIS.

Moriarty, P.J., Hansen, A.C., 2005. Aerodyn theory manual. National Renewable Energy Laboratory Technical Report. NREL/EL-500-36881.

Nezu, I., Nakagawa, H., 1993. Turbulence in Open-Channel Flows. IAHR/AIRH. A.A.Balkema-Rotterdam-Brookfield.

Nishino, T., Willden, R.H.J., 2013. Two-scale dynamics of flow past a partial cross-stream array of tidal turbines. Journal of Fluid Mechanics 730, 220–244.

Prandtl, L., 1927. Uber die ausgebildete turbulenz. Zeitschrift für angewandte Mathematik und Mechanik 5, 137–138.

Stallard, T.J., Collings, R., Feng., T., Whelan, J.I., 2013. Interactions between tidal turbine wakes: experimental study of a group of 3-bladed rotors. Philosophical Transactions of the Royal Society A 371, 2012.0159.

Stansby, P.K., 2003. A mixing length model for shallow turbulent wakes. Journal of Fluid Mechanics 495, 369–384.

Taylor, P.H., Santo, H., Choo, Y.S., 2013. Current blockage: reduced Morison forces on space frame structures with high hydrodynamic area, and in regular waves and current. Ocean Engineering 57, 11–24.

Vickery,B.J., 1965. On the flow behind a coarse grid and its use as a model of atmospheric turbulence in studies related to wind loads on buildings. Aero Report 1143, National Physical Laboratory.

Whelan, J.I., Stallard, T.J., 2011. Arguments for modifying the geometry of a scale model rotor. In: Bahaj, A.S. (Ed.), Proceedings of the 8th European Wave and Tidal Energy Conference, 5–9 September, Southampton, UK, p. on CD. Paper no. 50.